



## Research paper

# Nonplanar structure of $C_6H_5SCF_3$ facilitates $\pi\sigma^*$ -mediated photodissociation reaction on the $S_1$ state



So-Yeon Kim<sup>a</sup>, Jeongmook Lee<sup>a,c</sup>, Sang Kyu Kim<sup>a,\*</sup>, Young S. Choi<sup>b,\*</sup>

<sup>a</sup> Department of Chemistry, KAIST, Daejeon 305-701, Republic of Korea

<sup>b</sup> Department of Chemistry, Inha University, Incheon 402-751, Republic of Korea

<sup>c</sup> Nuclear Chemistry Research Division, Korea Atomic Energy Research Institute, Daejeon 305-353, Republic of Korea

## ARTICLE INFO

## Article history:

Received 8 June 2016

In final form 30 June 2016

Available online 30 June 2016

## Keywords:

Nonadiabatic transition

Conical intersection

Predissociation

## ABSTRACT

Vibrational structure of trifluoromethylthiobenzene ( $C_6H_5SCF_3$ ) on the  $S_1$  state has been investigated by resonance-enhanced two-photon ionization spectroscopy and nature of predissociation dynamics is inferred from homogeneously broadened spectral features. As  $C_6H_5SCF_3$  adopts a nonplanar structure in both the  $S_0$  and  $S_1$  states, the effective adiabatic barrier generated by avoided crossing of optically-bright bound  $S_1$  ( $\pi\pi^*$ ) and dark-repulsive  $S_2$  ( $\pi\sigma^*$ ) surfaces along the reaction coordinate is significantly lowered, giving the  $S_1$  lifetime of  $\sim 300$  fs. This experiment demonstrates that the molecular structure spanned by the reactive flux near the curve-crossing region dictates reaction rate as well as nonadiabatic transition probability.

© 2016 Elsevier B.V. All rights reserved.

## 1. Introduction

Relationship between molecular structure and chemical reactivity has long been one of the most challenging and important research topics in chemistry and biology. Despite a number of excellent theoretical and experimental related works to date, the structure-reactivity relationship at the molecular level is still beyond our full understanding. This is especially true for conformational isomers which are readily switchable by internal rotations around single bonds. As it is nontrivial to separate and identify different conformational isomers in ambient condition, conformation-dependent chemical reactivity has often been conjectured especially for complicated chemical or biological processes. On the other hand, however, when the molecule is cooled down sufficiently in the gas phase, it is in principle possible to separate different conformers by spectroscopic tools. Indeed, recent dynamics studies had shown that completely different reaction pathways are given for spectroscopically-selected different conformers in photodissociation reactions of 1-iodopropane [1] or 1-propanal ions [2]. Totally different dynamic releases of available energies in axial or equatorial conformers of iodocyclohexane [3] has also been reported. Recent studies demonstrating quite successful spatial separation of different conformers according their relative dipole moment strengths in the Stark-deflector give very

bright future in the conformer-selective dynamics researches, especially for neutral molecules and clusters [4,5].

In many cases, however, only one stable conformer is overwhelmingly populated in the molecular beam, and thus it hampers detailed conformer-specific dynamics studies. One of the ways avoiding this intrinsic limit would be the conformational tuning by the chemical substitution. Namely, if the electronic and nuclear configurations associated with a particular reaction pathway remain almost intact, it could be possible to make the whole molecule adopt different conformational structure from the bare species by the chemical substitution. For instance, it had been demonstrated that the dihedral angle of SH moiety of thiophenol with respect to the benzene moiety could be modified by the chemical substitution on the *para*-position of the ring [6]. As the SH dihedral angle with respect to the ring plane is so critical for the nonadiabatic transition probability in the proximity of planar conical intersections, nonadiabaticity may be controlled by the conformational manipulation of thiophenol induced by the chemical substitution. Actually, compared to the case of bare thiophenol where the SH moiety is parallel to the ring moiety, the nonadiabatic transition probability had been found to drastically decrease as the SH moiety becomes almost perpendicular to the ring when the methoxy group is substituted on the *para* position of thiophenol [7–13]. It should be noted, however, that conformer-specific dynamics are hardly expected to be prominent for slow reactions in general. This is because when the reactive flux undergoes significant energy randomization process prior to bond dissociation, the initial structural memory would be easily washed out.

\* Corresponding authors.

E-mail addresses: [sangkyukim@kaist.ac.kr](mailto:sangkyukim@kaist.ac.kr) (S.K. Kim), [yschoi@inha.ac.kr](mailto:yschoi@inha.ac.kr) (Y.S. Choi).

In recent works in our own group [14,15] and Ashfold/Stavros groups [16], it has been found that the S–CH<sub>3</sub> bond dissociation of the S<sub>1</sub> thioanisole is much slower compared to prompt S–H bond breakage of thiophenol at S<sub>1</sub>. Both thioanisole and thiophenol are planar at minimum energies of S<sub>0</sub> and S<sub>1</sub>, and their huge differences in S<sub>1</sub> lifetimes are attributed to the much larger reaction barrier height along the S–CH<sub>3</sub> bond elongation of thioanisole compared to that of thiophenol along the S–H bond elongation coordinate. Here on the excited states of thioanisole or thiophenol, the reaction barrier is the consequence of curve crossing of bound S<sub>1</sub> and repulsive S<sub>2</sub> states along the reaction coordinate. As the energy randomization process is not expected to be complete in the relatively shallow excited-state potential well, the reaction barrier is intrinsically dynamic. In other words, the excited-state reactive flux is not necessarily destined to follow the minimum energy reaction pathway where the saddle point is defined as a transition-state. Especially because the S<sub>1</sub>/S<sub>2</sub> conical intersection seam is planar, conformational change in terms of the SH or SCH<sub>3</sub> dihedral angle of thiophenol or thioanisole with respect to the ring moiety could be largely responsible for the dynamic change of the effective reaction barrier shape. In this work, the conformational preference has been largely modified by the chemical substitution of SCH<sub>3</sub> of thioanisole with SCF<sub>3</sub>, giving quite different conformer-specific excited-state dynamics. With the aid of *ab initio* calculations, we here demonstrate the importance of molecular conformation in the whole dynamics of excited-state reactions.

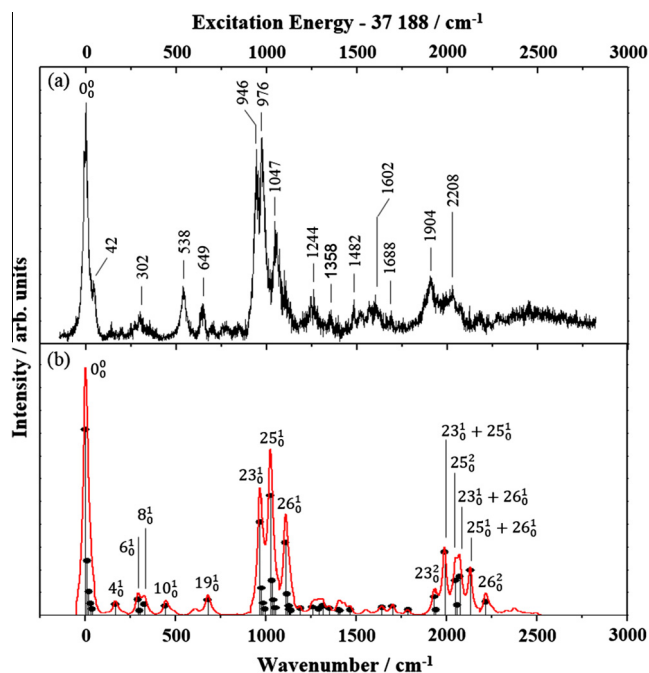
## 2. Experiment

Detailed experimental setup had been described in a previous work [17]. Trifluoromethylthiobenzene (TCI, ~97%) was heated to 90 °C before being seeded in the Ar carrier gas. The sample mixture was then expanded into vacuum through a nozzle orifice (General Valve Series 9, 0.5 mm diameter) with a backing pressure of ~2 atmosphere. The supersonic molecular beam passes through a 0.5 mm diameter skimmer (Beam Dynamics) before being intersected with UV laser pulse in the perpendicular geometry. To obtain resonant-enhanced two-photon ionization (R2PI) spectra, the laser pulse in 250–270 nm region was generated by frequency doubling of the dye laser (Spectra-Physics, Scanmate II) output pumped by the third harmonic of a Nd:YAG laser (Spectra-Physics, GCR-150). For the photoelectron imaging, the pump laser wavelength was fixed at the S<sub>1</sub> origin and the same laser pulse was used as a probe to generate photoelectrons. Photoelectrons were velocity-mapped onto the position sensitive detector (Burle, Ø = 40 mm) coupled to a personal-computer-interfaced CCD camera (Sony XC-ST50, 768 × 494 pixels). The obtained photoelectron image was reconstructed with a BASEX [18] algorithm using the IMACQ acquisition software [19].

All *ab initio* calculations were performed with Molpro and the Franck-Condon simulations were carried out using the FClab II program package [20,21]. Equilibrium configuration, relative energies, harmonic vibrational frequencies and potential energy cuts were calculated using the state-averaged complete active space self-consistent field (SA3-CASSCF(12,11)) with a 6-311\*\*G(d,p) basis set. Second order multi-reference perturbation calculation [22] (CASPT2, level shift = 0.4) was carried out at the equilibrium. The SA3-CASSCF(11,11)/6-311\*\*G(d,p) level of theory was used for the D<sub>0</sub> state calculation. Active spaces for each state are presented in the Table S1.

## 3. Results and discussion

R2PI spectrum of C<sub>6</sub>H<sub>5</sub>SCF<sub>3</sub> shows a strongly observed S<sub>1</sub>-S<sub>0</sub> origin at 37 188 cm<sup>-1</sup>, Fig. 1. The origin band is found to be homoge-



**Fig. 1.** S<sub>1</sub> – S<sub>0</sub> REMPI spectrum of jet cooled (trifluoromethylthio)benzene (a) and Franck-Condon simulated spectrum with appropriate vibrational mode assignment using unscaled SA3-CASSCF(12,11) vibrational frequencies (b). Comprehensive mode assignments are given in supplementary information.

neously broadened, giving the upper bound for the full width at half-maximum of ~33 cm<sup>-1</sup> corresponding to the lifetime of ~300 fs. This is surprising at the first glance since the S<sub>1</sub> lifetime of C<sub>6</sub>H<sub>5</sub>SCH<sub>3</sub> had been measured to be ~1.4 ns [16] and CH<sub>3</sub> to CF<sub>3</sub> substitution of thioanisole is not expected to influence excited-state dynamics much as two lowest electronic configurations of S<sub>1</sub> (ππ\*) and S<sub>2</sub> (πσ\*) are mainly associated with the C<sub>6</sub>H<sub>5</sub>S moiety. This is manifested by strongly observed ring expansion modes in the R2PI spectrum in the 940Z1050 cm<sup>-1</sup> region above the origin, indicating that the S<sub>1</sub>-S<sub>0</sub> optical transition mainly induces ring distortion modes whereas the structure of the SCF<sub>3</sub> moiety is little influenced. Calculated vertical and adiabatic excitation energies and corresponding oscillator strengths (*f*) for transitions from S<sub>0</sub> to the first (<sup>1</sup>ππ\*) and second (<sup>1</sup>nσ\*) electronically excited states are listed in Table 1. Theoretical value for the S<sub>1</sub>-S<sub>0</sub> adiabatic transition energy of 37916 cm<sup>-1</sup> (36459) with CASSCF (CASPT2) matches very well with the experimentally observed origin of 37 188 cm<sup>-1</sup>. Most of observed vibronic bands in the R2PI spectrum are appropriately assigned in terms of their frequencies and intensities using the Franck-Condon simulations based on *ab initio* molecular structure and harmonic vibrational frequency values, Fig. 1. All of bands are found to be broad and do not show any particular mode-dependency in their bandwidths. At high S<sub>1</sub> internal

**Table 1**  
Calculated adiabatic and vertical transition energies and oscillator strengths (*f*) for (trifluoromethylthio)benzene.

State	SA3-CASSCF(12,11)/6-311**G(d,p)			
	Transition <sup>a</sup>	Adiab. (eV)	Vert. (eV)	<i>f</i>
S <sub>1</sub>	<sup>1</sup> ππ*	4.70	4.92	0.0025
		(4.52) <sup>b</sup>	(4.72) <sup>b</sup>	
S <sub>2</sub>	<sup>1</sup> nσ*	–	6.16 (5.35) <sup>b</sup>	0.0015

<sup>a</sup> π\* and σ\* are configurationally mixed in antibonding orbitals.

<sup>b</sup> Values in parentheses are obtained with CASPT2 correction.

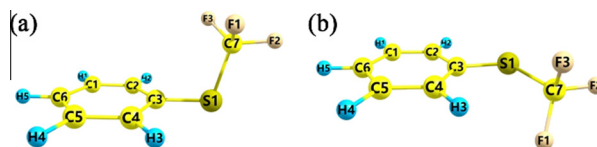
energies above  $2000\text{ cm}^{-1}$ , broad featureless background signal starts to emerge and this may be ascribed to spectral congestion caused by the increase of the density of states. Unresolved peaks weakly-observed at the blue shoulder of the origin might be attributed to the  $\text{SCF}_3$  dihedral torsional mode excitation.

Origin for the ultrashort  $S_1$  lifetime of  $\text{C}_6\text{H}_5\text{SCF}_3$  could be found from the large conformational change of thioanisole upon the methyl group fluorination. Indeed, the most notable structural change by the  $\text{CH}_3$  to  $\text{CF}_3$  substitution of thioanisole is the dihedral torsional angle of  $\text{SCF}_3$  moiety with respect to the ring. From the previous gas electron diffraction study [23], it had been reported that fluorination of the methyl group of thioanisole gives rise to the conformational change from planar to perpendicular orientation of  $\text{S}-\text{CH}_3(\text{CF}_3)$  bond relative to the benzene ring. Consistently, according to our SA3-CASSCF calculations,  $\text{C}_6\text{H}_5\text{SCF}_3$  adopts non-planar geometry at minimum energies of both  $S_0$  and  $S_1$ , giving  $\sim 91^\circ$  dihedral angle of  $\text{SCF}_3$  with respect to ring, Table 2. Generally speaking, in the  $\pi\sigma^*$ -mediated photodissociation pathways of thioanisoles, two conical intersections are encountered along the  $\text{S}-\text{CH}_3$  bond elongation coordinate [14–16]. The first one results from curve crossing of the optically-bright bound  $S_1$  ( $\pi\pi^*$ ) and dark repulsive  $S_2$  ( $\pi\sigma^*$ ). At the later stage of reaction,  $S_2$  crosses with  $S_0$  giving the second conical intersection at the planar geometry. At the asymptotic limit,  $S_2$  diabatically correlates to the ground-

state  $\text{C}_6\text{H}_5\text{S}(\tilde{\text{X}})$  radical whereas  $S_0$  correlates to the excited state  $\text{C}_6\text{H}_5\text{S}(\tilde{\text{A}})$  radical diabatically. In other words, the reactive flux on  $S_2$  follows the adiabatic path to give the  $\text{C}_6\text{H}_5\text{S}(\tilde{\text{A}})$  fragment whereas  $\text{C}_6\text{H}_5\text{S}(\tilde{\text{X}})$  is produced only by the nonadiabatic transition at the second conical intersection. Potential energy surfaces of  $\text{C}_6\text{H}_5\text{SCF}_3$  calculated along the  $\text{S}-\text{CF}_3$  bond elongation coordinate give the similar shapes to those of thioanisole, Fig. 2. It should be noted, however, that conical intersections are not evident in this case as  $\text{C}_6\text{H}_5\text{SCF}_3$  adopts the perpendicular orientation at both  $S_0$  and  $S_1$ , and the perpendicular orientation is maintained as the  $\text{S}-\text{CF}_3$  bond length is elongated in the calculation. Namely, due to avoided crossing at the perpendicular orientation, adiabatic potential energy surfaces are somewhat isolated to each other even though pseudo conical intersection seam could be present at the perpendicular orientation. The adiabatic reaction barrier of the  $S_1$  potential well is calculated to be  $1437\text{ cm}^{-1}$  according to our calculation. Supposed that the reaction coordinate is parallel with the  $\text{S}-\text{CF}_3$  stretching mode ( $\sim 813\text{ cm}^{-1}$ ), the effective barrier from the zero-point level would be  $\sim 1030\text{ cm}^{-1}$  [24]. This is much lower than the adiabatic reaction barrier of  $3469\text{ cm}^{-1}$  calculated for thioanisole at the planar geometry for the  $\text{S}-\text{CH}_3$  bond dissociation although it may not be straightforward to directly compare the potential energy surface of  $\text{C}_6\text{H}_5\text{SCF}_3$  with that of  $\text{C}_6\text{H}_5\text{SCH}_3$  as

**Table 2**

Calculated molecular structural parameters and minimum energies for the ground ( $S_0$ ), the first excited ( $S_1$ ), and cationic ground ( $D_0$ ) states. Geometries for (a)  $S_0$ ,  $S_1$  and (b)  $D_0$ .

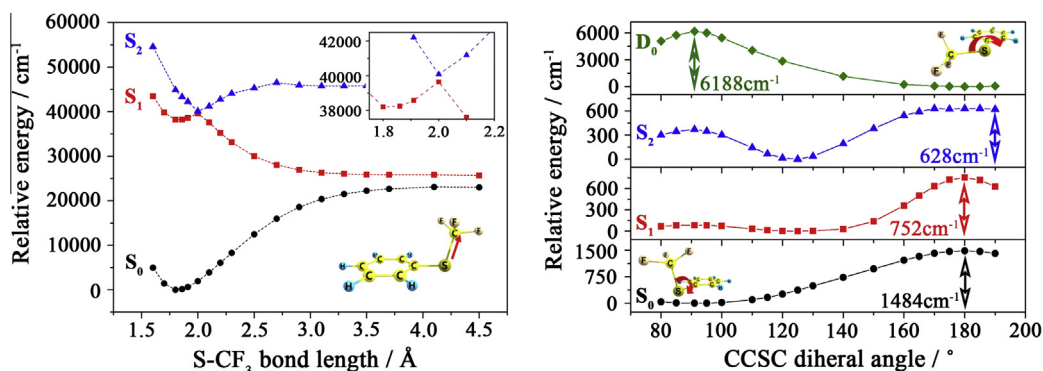


	Equilibrium		
	$S_0$	$S_1$	$D_0$
Relative energy ( $\text{cm}^{-1}$ )	0 (0) <sup>c</sup>	37916 (36459) <sup>c</sup>	39666 <sup>a</sup> (38072) <sup>c</sup>
$d(\text{C3}-\text{S1})$ (Å)	1.81	1.79	1.73
$d(\text{S1}-\text{C7})$ (Å)	1.86	1.87	1.90
$\gamma(\text{C3}-\text{S1}-\text{C7})$ ( $^\circ$ )	101.81	102.02	105.83
$\gamma(\text{S1}-\text{C7}-\text{F2})$ ( $^\circ$ )	107.58	107.74	105.03
$\delta(\text{C2}-\text{C3}-\text{S1}-\text{C7})$ ( $^\circ$ )	91.26	90.89	0
$d(\text{C}-\text{C})$ (Å) <sup>b</sup>	1.40	1.43	1.40
$d(\text{C3}-\text{C6})$ (Å)	2.79	2.88	2.78

<sup>a</sup> The  $S_1 - S_0$  vertical excitation energy at the  $S_0$  minimum geometry.

<sup>b</sup> Averaged values for the phenyl moiety.

<sup>c</sup> The values in parentheses are obtained with CASPT2 correction.



**Fig. 2.** Three lowest ( $S_0$ ,  $S_1$ , and  $S_2$ ) adiabatic potential energy cuts along  $\text{S}-\text{CF}_3$  bond elongation coordinate obtained by SA3-CASSCF(12,11) level of theory (left) and the potential energy cuts along CCSC dihedral angle for  $S_0$ ,  $S_1$ ,  $S_2$  and  $D_0$  states (right) with the CASPT2 correction.

associated electronic configurations are not expected to be intact upon fluorination. And yet, the perpendicular orientation of the S—CF<sub>3</sub> bond relative to the ring of C<sub>6</sub>H<sub>5</sub>SCF<sub>3</sub> facilitates the dissipation process of S<sub>1</sub> by lowering the effective adiabatic barrier to the major dissociation channel due to the increase of the coupling matrix term values in the avoided crossing. It seems to be thus reasonable to state that thioanisole undergoes the dramatic conformational change (planar to perpendicular) upon fluorination of the photo-labile methyl-group and this conformational change makes lower the adiabatic barrier to the escape of the reactive flux from the shallow S<sub>1</sub> potential well along the S—CF<sub>3</sub> bond dissociation coordinate.

Importantly, it is interesting to note that the perpendicular orientation of SCF<sub>3</sub> to the ring influences electronic configurations of S<sub>1</sub> and S<sub>2</sub>. Indeed, from our molecular-orbital calculations, the extent of electronic conjugation between benzyl ring  $\pi$  ( $\pi^*$ ) and S—CF<sub>3</sub>  $\sigma$  ( $\sigma^*$ ) orbitals is predicted to be significant in the perpendicular geometry of C<sub>6</sub>H<sub>5</sub>SCF<sub>3</sub>, which makes the S<sub>1</sub> state to be more efficiently coupled to the repulsive S<sub>2</sub> as a consequence of the significant electronic configurational mixings in orbitals involved in optical and nonradiative transitions (supplementary information). Another notable interesting factor is the non-rigidity of the perpendicular configuration of the S<sub>1</sub> C<sub>6</sub>H<sub>5</sub>SCF<sub>3</sub> along the dihedral torsional coordinate. For instance, the barrier height along the CCSC dihedral angle calculated to be 1484 cm<sup>-1</sup> for S<sub>0</sub> is predicted to be 752 cm<sup>-1</sup> for S<sub>1</sub> state. Actually, this is a bit higher than previously reported value of 2.4–2.6 kcal/mol obtained from B3LYP or MP2 calculations [23]. Calculated barrier height especially along the torsional angle is known to be strongly subject to theoretical methods and basis sets, and our values here leave room for much improvement. It is still interesting though to note that potential energy curves along this conformational coordinate are calculated to be quite flat at minimum energy structures, giving 5 cm<sup>-1</sup> for the torsional frequency at S<sub>1</sub>, Fig. 2. This suggests that C<sub>6</sub>H<sub>5</sub>SCF<sub>3</sub> in the S<sub>1</sub> state is floppy at least in terms of the SCF<sub>3</sub> dihedral angle with respect to the ring. As stated above, the dynamic reaction barrier shape resulting from avoided crossing of S<sub>1</sub> and S<sub>2</sub> is sensitive to the SCF<sub>3</sub> dihedral angle. The potential well against the S—CF<sub>3</sub> bond dissociation path is then expected to be dynamically influenced as the SCF<sub>3</sub> dihedral angle is being changed, giving the fluctuating barrier for the adiabatic path. Theoretical prediction that the molecule at S<sub>1</sub> is floppy along the dihedral angle, therefore, suggests that the effective reaction barrier to the S—CF<sub>3</sub> bond cleavage could also be dynamically floppy, expediting the bond dissociation process. This also supports our experimental observation

of the ultrashort S<sub>1</sub> lifetime of the title molecule. Conical intersections are not searched for this system at the present time.

Finally, photoelectron image taken from (1 + 1) two-photon ionization via the S<sub>1</sub> origin as an intermediate state shows broad structureless feature, Fig. 3. This is indicative of the large structural change upon ionization. This is consistent with our calculations, predicting that the cationic ground state of C<sub>6</sub>H<sub>5</sub>SCF<sub>3</sub> adopts the planar orientation of the SCF<sub>3</sub> group relative to the benzene ring, Fig. 2. Therefore, vertical ionization gives rise to much vibrational excitation presumably of the dihedral torsional mode.

#### 4. Conclusions

The conformational change of thioanisole upon the methyl-group fluorination in terms of the dihedral angle of the S—CH<sub>3</sub>(CF<sub>3</sub>) bond with respect to the benzene ring influences the  $\pi\sigma^*$ -mediated predissociation dynamics. Namely the perpendicular orientation of the SCF<sub>3</sub> moiety relative to the ring significantly lowers the effective adiabatic reaction barrier height, giving the S<sub>1</sub> lifetime of  $\sim$ 300 fs. This experiment demonstrates that molecular conformational change induced by chemical substitution, if it is critically involved in the state-coupling near the curve-crossing region, dictates reaction rates as well as nonadiabatic transition probability.

#### Acknowledgement

This work was financially supported by National Research Foundation in Korea (NRF) (2015R1A2A1A01004470).

#### Appendix A. Supplementary material

Supplementary data associated with this article can be found, in the online version, at <http://dx.doi.org/10.1016/j.cplett.2016.06.083>.

#### References

- [1] S.T. Park, S.K. Kim, M.S. Kim, Observation of conformation-specific pathways in the photodissociation of 1-iodopropane ions, *Nature* 415 (2002) 306.
- [2] M.H. Kim, L. Shen, H. Tao, T.J. Martinez, A.G. Suits, Conformationally controlled chemistry: excited-state dynamics dictate ground-state reaction, *Science* 315 (2007) 1561.
- [3] X. Zheng, C.W. Lee, D.L. Phillips, Resonance Raman study of the A-band short-time photodissociation dynamics of axial and equatorial conformers of iodyclopentane, *J. Chem. Phys.* 111 (1999) 11034.
- [4] F. Filsinger, J. K pper, G. Meijer, J.L. Hansen, J. Maurer, J.H. Nielsen, L. Holmegaard, H. Stapelfeldt, Pure samples of individual conformers: the separation of stereoisomers of complex molecules using electric fields, *Angew. Chem. Int.* 48 (2009) 6900.
- [5] T. Kierspel, D.A. Horke, Y.P. Chang, J. K pper, Spatially separated polar samples of the cis and trans conformers of 3-fluorophenol, *Chem. Phys. Lett.* 591 (2014) 130.
- [6] P. Mulder, O. Mozenson, S. Lin, C.E.S. Bernardes, M.E. Minas da Piedade, A.F.L.O. M. Santos, M.A.V. Ribeiro da Silva, G.A. Dilabio, H.G. Korth, K.U. Ingold, Effect of ring substitution on the S—H bond dissociation enthalpies of thiophenols, an experimental and computational study, *J. Phys. Chem. A* 110 (2006) 9949.
- [7] J.S. Lim, I.S. Lim, K.S. Lee, D.S. Ahn, Y.S. Lee, S.K. Kim, Intramolecular orbital alignment observed in the photodissociation of [D1] thiophenol, *Angew. Chem. Int.* 45 (2006) 6290.
- [8] J.S. Lim, Y.S. Lee, S.K. Kim, Control of intramolecular orbital alignment in the photodissociation of thiophenol: conformational manipulation by chemical substitution, *Angew. Chem. Int.* 47 (2008) 1853.
- [9] I.S. Lim, J.S. Lim, Y.S. Lee, S.K. Kim, Experimental and theoretical study of the photodissociation reaction of thiophenol at 243 nm: intramolecular orbital alignment of the phenylthiyl radical, *J. Chem. Phys.* 126 (2007) 034306.
- [10] J.S. Lim, H. Choi, I.S. Lim, S.B. Park, Y.S. Lee, S.K. Kim, Photodissociation dynamics of Thiophenol-d1: the nature of excited electronic states along the S—D bond dissociation coordinate, *J. Phys. Chem. A* 113 (2009) 10410.
- [11] A.L. Devine, M.G.D. Nix, R.N. Dixon, M.N.R. Ashfold, Near-ultraviolet photodissociation of thiophenol, *J. Phys. Chem. A* 112 (2008) 9563.
- [12] M.N.R. Ashfold, A.L. Devine, R.N. Dixon, G.A. King, M.G.D. Nix, T.A.A. Oliver, Exploring nuclear motion through conical intersections in the UV photodissociation of phenols and thiophenol, *Proc. Natl. Acad. Sci. U.S.A.* 105 (2008) 12701.

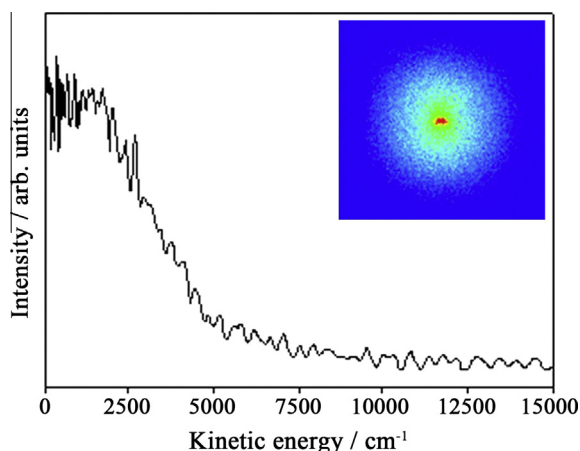


Fig. 3. Photoelectron image (inset) and its kinetic energy spectrum taken via S<sub>1</sub> origin (37188 cm<sup>-1</sup>) as an intermediate state.

- [13] G.M. Roberts, A.S. Chatterley, J.D. Young, V.G. Stavros, Diffusion coefficients from  $^{13}\text{C}$  PGSE NMR measurements—fluorine-free ionic liquids with the DCTA-anion, *J. Phys. Chem. Lett.* 3 (2012) 348.
- [14] J.S. Lim, S.K. Kim, Experimental probing of conical intersection dynamics in the photodissociation of thioanisole, *Nat. Chem.* 2 (2010) 627.
- [15] S. Han, J.S. Lim, J.H. Yoon, J. Lee, S.Y. Kim, S.K. Kim, Conical intersection seam and bound resonances embedded in continuum observed in the photodissociation of thioanisole-d<sub>3</sub>, *J. Chem. Phys.* 140 (2014) 054307.
- [16] G.M. Roberts, D.J. Hadden, L.T. Bergendahl, A.M. Wenge, S.J. Harris, T.N.V. Karsili, M.N.R. Ashfold, M.J. Paterson, V.G. Stavros, Exploring quantum phenomena and vibrational control in  $\sigma^*$  mediated photochemistry, *Chem. Sci.* 4 (2013) 993.
- [17] D.-S. Ahn, J. Lee, Y.C. Park, Y.S. Lee, S.K. Kim, Nuclear motion captured by the slow electron velocity imaging technique in the tunnelling predissociation of the S1 methylamine, *J. Chem. Phys.* 136 (2012) 024306.
- [18] V. Dribinski, A. Ossadtchi, V.A. Mandelshtam, H. Reisler, Reconstruction of Abel-transformable images: the gaussian basis-set expansion Abel transform method, *Rev. Sci. Instrum.* 73 (2002) 2634.
- [19] W. Li, S.D. Chambreau, S.A. Lahankar, A.G. Suits, Megapixel ion imaging with standard video, *Rev. Sci. Instrum.* 76 (2005) 063106.
- [20] I. Pugliesi, K. Müller-Dethlefs, The use of multidimensional Franck-Condon simulations to assess model chemistries: a case study on phenol, *J. Phys. Chem. A* 110 (2006) 4657.
- [21] All Franck-Condon simulations have been carried out using FC-LabII Version 2009a, a computational package developed by C. Schrieffer, M.C.R. Cockett and I. Pugliesi. The latest information on program updates, a basic introduction to Franck-Condon simulations and a free download of the software can be found at <<http://www.fclab2.net/>>.
- [22] P. Celani, H.-J. Werner, Multireference perturbation theory for large restricted and selected active space reference wave functions, *Chem. Phys.* 112 (2000) 5546.
- [23] I.F. Shishkov, L.V. Khristenko, A.N. Rykov, L.V. Vilkov, G.V. Giricheva, H. Oberhammer, Structure and conformation of (trifluoromethyl)thiobenzene, *C<sub>6</sub>H<sub>5</sub>SCF<sub>3</sub>*: gas electron diffraction and quantum chemical calculations, *J. Mol. Struct.* 876 (2008) 147.
- [24] R.J. Le Roy, W.K. Liu, Energies and widths of quasibound levels (orbiting resonances) for spherical potentials, *J. Chem. Phys.* 69 (1978) 3622.

**Supporting Information for:**

**Nonplanar structure of C<sub>6</sub>H<sub>5</sub>SCF<sub>3</sub> facilitates  
 $\pi\sigma^*$ -mediated photodissociation reaction on the S<sub>1</sub> state**

So-Yeon Kim, Jeongmook Lee<sup>§</sup>, and Sang Kyu Kim\*

*Department of chemistry, KAIST, Daejeon 305-701, Republic of Korea.*


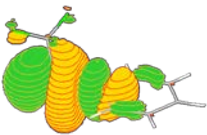
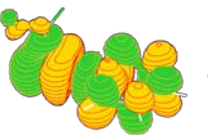
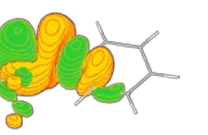



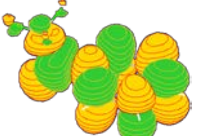
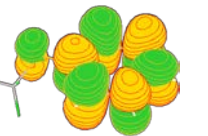


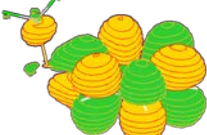
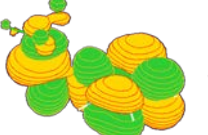
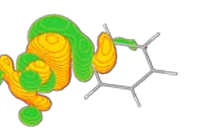

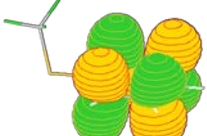
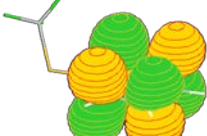
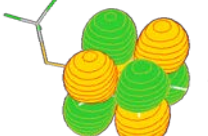
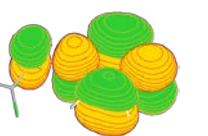




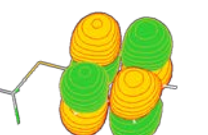

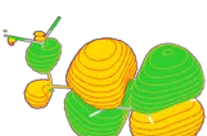
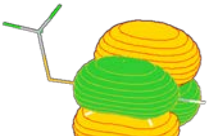

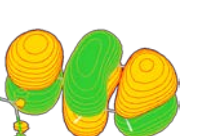

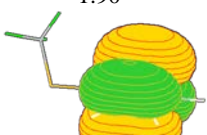

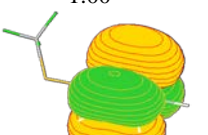
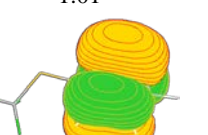

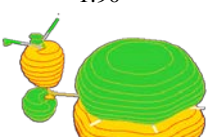
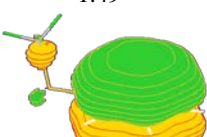

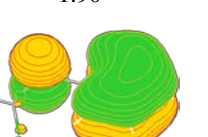

Young S. Choi\*

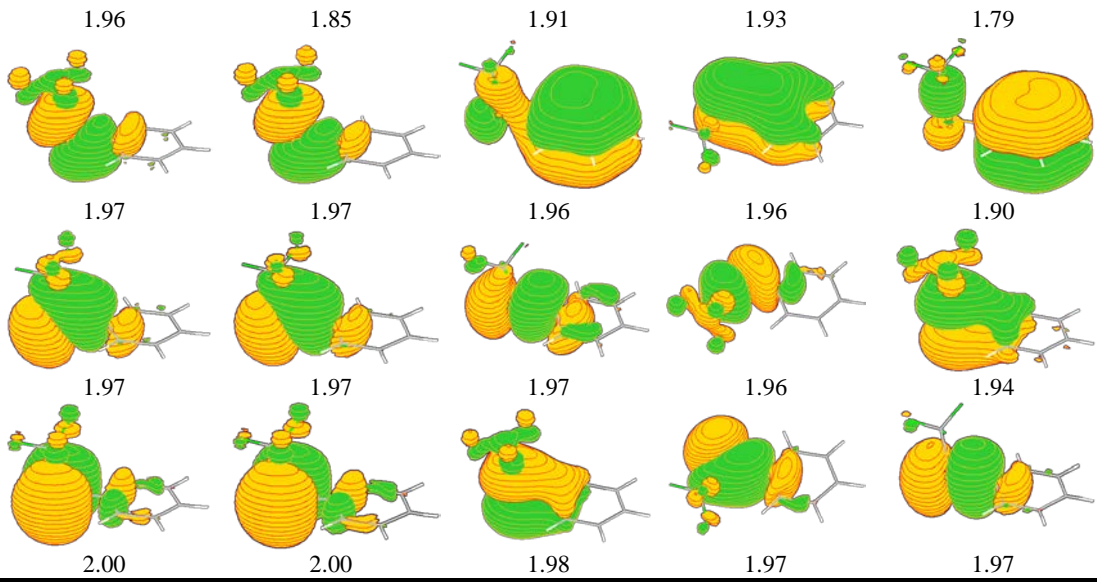
*Department of Chemistry, Inha University, Incheon 402-751, Republic of Korea*

\*E-mail: [sangkyukim@kaist.ac.kr](mailto:sangkyukim@kaist.ac.kr) (SKK), [yschoi@inha.ac.kr](mailto:yschoi@inha.ac.kr) (YSC)

<sup>§</sup>*Nuclear Chemistry Research Division, Korea Atomic Energy Research Institute, Daejeon 305- 353,  
Korea*

**Table S1.** Molecular orbital (MO) diagrams and associated occupation numbers (Occ) for  $S_0$ ,  $S_1$ ,  $S_2$  and  $D_0$  of (trifluoromethylthio)benzene at each equilibrium geometry and  $S$ -CF<sub>3</sub> elongated geometry (at  $R_{S-CF_3}=2.07\text{\AA}$ ) corresponding to the highest barrier on adiabatic  $S_1$  PEC. The MOs are obtained using SA3-CASSCF(12,11)/6-311<sup>++</sup>G(d,p) level of calculations for  $S_0$  and  $S_1$  states. And SA3-CASSCF(11,11)/6-311<sup>++</sup>G(d,p) for  $D_0$ . The MOs of repulsive  $S_2$  state are obtained by vertical excitation method with  $S_0$  equilibrium geometry

	$S_0$	$S_1$	$S_2$	$D_0$	Adiabatic barrier on $S_1$ PEC
MO					
Occ	0.03	0.03	0.04	0.03	0.03
					
	0.03	0.03	0.04	0.03	0.08
					
	0.04	0.12	0.10	0.04	0.23
					
	0.10	0.51	0.11	0.07	0.34
					
	0.10	0.64	1.00	0.09	0.67
					
	1.90	1.38	1.00	1.01	1.39
					
	1.90	1.49	1.90	1.90	1.66
					





**Table S2.** Calculated ( $S_0$ ,  $S_1$ , and  $D_0$ ) vibrational frequencies ( $\text{cm}^{-1}$ ) of (trifluoromethylthio)-benzene. The frequencies are obtained from the SA3-CASSCF(12,11)/6-311++G(d,p) level of calculation for  $S_0$  and  $S_1$  and SA3-CASSCF(11,11)/6-311++G(d,p) for  $D_0$ .

Mode <sup>a</sup>	$S_0$ ( $C_1$ ) Freq.		$S_1$ ( $C_1$ ) Freq.			$D_0$ ( $C_s$ ) Freq.		
	Calc.	Mode <sup>b</sup>	Calc.	Expt. <sup>c</sup>	Mode <sup>b</sup>	Calc.	Symm.	Mode <sup>b</sup>
$\nu_1$	33	$\tau$	5	$11(\nu_1^2)$	$\tau$	58	a''	$\tau\text{CF}_3$
$\nu_2$	49	$\tau\text{CF}_3$	42		$\tau\text{CF}_3$	72	a''	$\tau$
$\nu_3$	76	$\beta_s\text{CSC}$	57		$\beta_s\text{CSC}$	121	a'	$\beta_s\text{CSC}$
$\nu_4$	209	10b	165		10b	160	a''	10b
$\nu_5$	274	9b <sup>d</sup>	266		9b <sup>d</sup>	257	a'	9b <sup>d</sup>
$\nu_6$	299	$\beta_s\text{CF}$	291	(302) <sup>e</sup>	$\beta_s\text{CF}$	297	a'	$\beta_s\text{CF}$
$\nu_7$	362	$\gamma_{as}\text{CF}_2$	300		16a	331	a''	$\gamma_{as}\text{CF}_2$
$\nu_8$	436	16b	326		16b	401	a''	16a
$\nu_9$	437	16a	357		$\gamma_{as}\text{CF}_2$	459	a''	16b
$\nu_{10}$	464	6a	442	538	6a	471	a'	6a
$\nu_{11}$	516	$M^f$	452		4	485	a'	$M^f$
$\nu_{12}$	593	$\gamma_{as}\text{CF}_3$	499		$M^f$	597	a''	$\gamma_{as}\text{CF}_3$
$\nu_{13}$	614	$\beta_s\text{CF}_2$	569		11	612	a'	$\beta_s\text{CF}_2$
$\nu_{14}$	661	6b	590		$\gamma_{as}\text{CF}_3$	615	a'	6b
$\nu_{15}$	695	4	596		6b	639	a''	4
$\nu_{16}$	741	7a	615		$\beta_s\text{CF}_2$	741	a'	7a
$\nu_{17}$	769	11	635		10a	783	a''	11
$\nu_{18}$	816	$\beta_s\text{CF}_3^g$	649		17b	827	a'	$\beta_s\text{CF}_3^g$
$\nu_{19}$	872	10a	677	649	7a	852	a''	10a
$\nu_{20}$	945	17b	704		5	985	a''	17b
$\nu_{21}$	1001	17a	718		17a	1032	a'	12
$\nu_{22}$	1010	5	813		$\beta_s\text{CF}_3^g$	1036	a''	17a
$\nu_{23}$	1056	1	965	946	1	1044	a''	5
$\nu_{24}$	1094	12	1003		19b	1065	a'	1
$\nu_{25}$	1144	19b	1024	976	12	1160	a'	19a
$\nu_{26}$	1163	19a	1107	1047	19a	1167	a'	19b
$\nu_{27}$	1211	14	1226		$\nu_{sS}\text{-CF}_3^g$	1199	a'	$\nu_{sS}\text{-CF}_3^g$
$\nu_{28}$	1230	$\nu_{sS}\text{-CF}_3^g$	1244		14	1247	a'	14
$\nu_{29}$	1271	9a	1248		9a	1304	a'	9a
$\nu_{30}$	1319	15	1331		$\nu_{as}\text{CF}_2^h$	1399	a'	3
$\nu_{31}$	1333	$\nu_{as}\text{CF}_2^h$	1349		$\nu_s\text{CF}^h$	1407	a''	$\nu_{as}\text{CF}_2^h$
$\nu_{32}$	1348	$\nu_s\text{CF}^h$	1386		3	1445	a'	$\nu_s\text{CF}^h$
$\nu_{33}$	1432	3	1491		18b	1461	a'	15
$\nu_{34}$	1560	18b	1532		18a	1538	a'	18b
$\nu_{35}$	1611	18a	1623		8b	1590	a'	18a
$\nu_{36}$	1696	8b	1661		8a	1644	a'	8b
$\nu_{37}$	1719	8a	1862		15	1727	a'	8a
$\nu_{38}$	3320	13	3343		13	3347	a'	20a
$\nu_{39}$	3331	7b	3349		7b	3356	a'	13
$\nu_{40}$	3343	20a	3363		20a	3366	a'	7b
$\nu_{41}$	3355	20b	3370		20b	3374	a'	2
$\nu_{42}$	3358	2	3377		2	3409	a'	20b

<sup>a</sup> The modes are listed in the increasing order of vibrational frequencies.

<sup>b</sup> Normal modes are labeled according to the Ref. [22].

<sup>c</sup> The vibrational modes observed in the REMPI spectrum are presented in Expt. column.

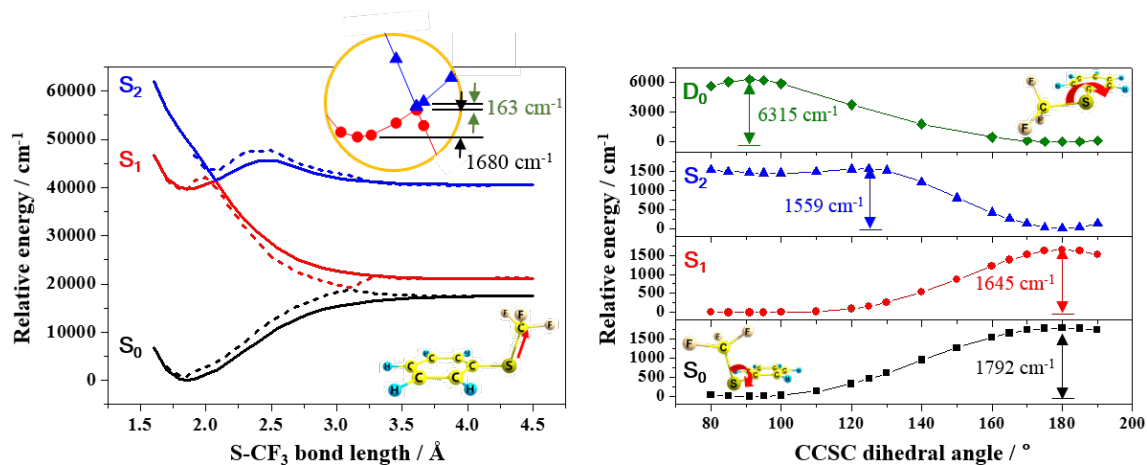
<sup>d</sup> Tentatively assigned.

<sup>e</sup> The  $\nu_6(\beta_s\text{CF})$ ,  $\nu_7(16a)$ , and  $\nu_8(16b)$  modes of  $S_1$  state are unresolved in REMPI spectra and present the broader peak shape because of the overlap.

<sup>f</sup> The mode is described in mixed motion with 16b,  $\beta_s\text{CSC}$  and  $\beta_s\text{CF}_2$ .

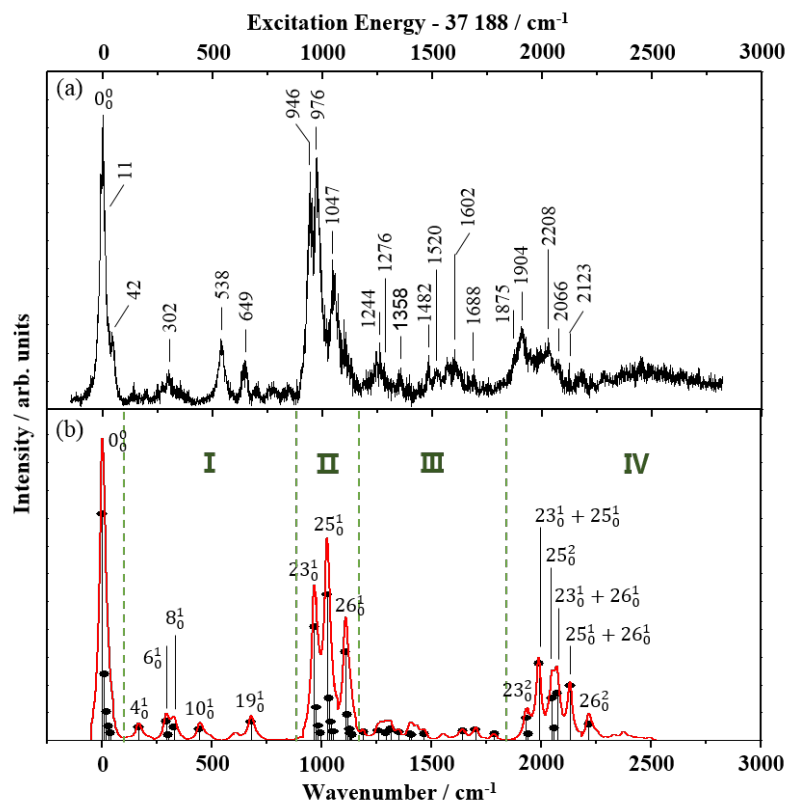
<sup>g</sup> The  $\beta_s\text{CF}_3$  and  $\nu_{sS}\text{-CF}_3$  modes are coupled.

<sup>h</sup> The stretching modes are generated by C atom's vibration mainly, not F atoms.



**Figure S1.** Three lowest ( $S_0$ ,  $S_1$ , and  $S_2$ ) adiabatic potential energy cuts along S-CF<sub>3</sub> bond elongation coordinate (left). Solid (dashed) lines adopt non-planar (planar) geometry. Potential energy cuts along CCSC dihedral angle for  $S_0$ ,  $S_1$ ,  $S_2$  and  $D_0$  states (right). All values are obtained by SA3-CASSCF(12,11) level of theory.

**Table S3.** Experimental, simulated vibrational frequencies and assignments for REMPI spectrum. All values are given in  $\text{cm}^{-1}$  units.



	Expt.	FC simulation <sup>a</sup>	Assignment	Description <sup>b</sup>
	(31 788)	(0)	$0_0^0$	-
I	11	9	$1_0^1$	$\tau$
	46	37	$1_0^8$	$\tau$
	302 <sup>c</sup>	291	$6_0^1$	SC F <sub>(2)</sub> bend.
		326	$8_0^1$	oop ring deform. (16b)
	538	442	$10_0^1$	S-C <sub>(7)</sub> stretch. + C <sub>(3)</sub> -S stretch. +CSC deform. (6a)
	649	677	$19_0^1$	C <sub>(3)</sub> -S stretch + ip ring deform. (7a)
II	946	965	$23_0^1$	ring stretch. (1)
	976	1024	$25_0^1$	ip ring deform. (12)
	1047	1107	$26_0^1$	ip ring deform. (19a)
III	1244 <sup>c</sup>	1256	$23_0^1 + 6_0^1$	
		1291	$23_0^1 + 8_0^1$	
	1276 <sup>c</sup>	1315	$25_0^1 + 6_0^1$	
		1350	$25_0^1 + 8_0^1$	
	1358	1399	$26_0^1 + 6_0^1$	
	1482	1407	$23_0^1 + 10_0^1$	
	1520	1466	$25_0^1 + 10_0^1$	
1602	1642	$23_0^1 + 19_0^1$		
1688	1785	$26_0^1 + 19_0^1$		
IV	1875	1930	$23_0^2$	
	1904	1988	$23_0^1 + 25_0^1$	
	2208	2072	$23_0^1 + 26_0^1$	
	2066	2131	$25_0^1 + 26_0^1$	
	2123	2215	$26_0^2$	

<sup>a</sup> SA3-CASSCF(12,11)/6-311<sup>++</sup>G(d,p) harmonic vibrational frequencies using MOLPRO were used.

<sup>b</sup> ip, in-plane; oop, out-of-plane; as, asymmetric. Corresponding Wilson's notations are denoted in parentheses.

<sup>c</sup> unresolved because of the overlap of the two broad peaks and small energy difference between  $6_0^1$  and  $8_0^1$ .

**Table S4.** Theoretical frequencies and Franck-Condon factors observed in the simulated spectrum presented in Figure 2.

	Calc. <sup>a</sup>	Expt. <sup>b</sup>	FC <sup>c</sup>	Assignment <sup>d</sup>
I	(0)	(31 788)	0.163	0 <sub>0</sub> <sup>0</sup>
	9	11	0.047	1 <sub>0</sub> <sup>2</sup>
	19		0.020	1 <sub>0</sub> <sup>4</sup>
	28		0.010	1 <sub>0</sub> <sup>6</sup>
	37	46	0.005	1 <sub>0</sub> <sup>8</sup>
	165		0.010	4 <sub>0</sub> <sup>1</sup>
	291	302 <sup>e</sup>	0.014	6 <sub>0</sub> <sup>1</sup>
	300		0.004	1 <sub>0</sub> <sup>2</sup> 6 <sub>0</sub> <sup>1</sup>
	326		0.010	8 <sub>0</sub> <sup>1</sup>
	442	538	0.008	10 <sub>0</sub> <sup>1</sup>
677	649	0.013	19 <sub>0</sub> <sup>1</sup>	
II	965	946	0.082	23 <sub>0</sub> <sup>1</sup>
	974		0.024	23 <sub>0</sub> <sup>1</sup> 1 <sub>0</sub> <sup>2</sup>
	983		0.010	23 <sub>0</sub> <sup>1</sup> 1 <sub>0</sub> <sup>4</sup>
	993		0.005	23 <sub>0</sub> <sup>1</sup> 1 <sub>0</sub> <sup>4</sup>
	1024	976	0.105	25 <sub>0</sub> <sup>1</sup>
	1033		0.031	25 <sub>0</sub> <sup>1</sup> 1 <sub>0</sub> <sup>2</sup>
	1042		0.013	25 <sub>0</sub> <sup>1</sup> 1 <sub>0</sub> <sup>4</sup>
	1051		0.007	25 <sub>0</sub> <sup>1</sup> 1 <sub>0</sub> <sup>6</sup>
	1107	1047	0.064	26 <sub>0</sub> <sup>1</sup>
	1117		0.019	26 <sub>0</sub> <sup>1</sup> 1 <sub>0</sub> <sup>2</sup>
	1126		0.008	26 <sub>0</sub> <sup>1</sup> 1 <sub>0</sub> <sup>4</sup>
	1130		0.005	23 <sub>0</sub> <sup>1</sup> 4 <sub>0</sub> <sup>1</sup>
	1135		0.004	26 <sub>0</sub> <sup>1</sup> 1 <sub>0</sub> <sup>6</sup>
III	1189		0.006	25 <sub>0</sub> <sup>1</sup> 4 <sub>0</sub> <sup>1</sup>
	1256		0.007	23 <sub>0</sub> <sup>1</sup> 6 <sub>0</sub> <sup>1</sup>
	1291		0.005	23 <sub>0</sub> <sup>1</sup> 8 <sub>0</sub> <sup>1</sup>
	1315		0.008	25 <sub>0</sub> <sup>1</sup> 6 <sub>0</sub> <sup>1</sup>
	1350		0.006	25 <sub>0</sub> <sup>1</sup> 8 <sub>0</sub> <sup>1</sup>
	1399		0.005	26 <sub>0</sub> <sup>1</sup> 6 <sub>0</sub> <sup>1</sup>
	1407		0.004	23 <sub>0</sub> <sup>1</sup> 10 <sub>0</sub> <sup>1</sup>
	1466		0.005	25 <sub>0</sub> <sup>1</sup> 10 <sub>0</sub> <sup>1</sup>
	1642		0.007	23 <sub>0</sub> <sup>1</sup> 19 <sub>0</sub> <sup>1</sup>
	1701		0.008	25 <sub>0</sub> <sup>1</sup> 19 <sub>0</sub> <sup>1</sup>
1785		0.005	26 <sub>0</sub> <sup>1</sup> 19 <sub>0</sub> <sup>1</sup>	
IV	1930	1875	0.016	23 <sub>0</sub> <sup>2</sup>
	1939		0.005	23 <sub>0</sub> <sup>2</sup> 1 <sub>0</sub> <sup>2</sup>
	1988	1904	0.056	23 <sub>0</sub> <sup>1</sup> 25 <sub>0</sub> <sup>1</sup>
	2047		0.031	25 <sub>0</sub> <sup>2</sup>
	2056		0.009	25 <sub>0</sub> <sup>2</sup> 1 <sub>0</sub> <sup>2</sup>
	2072	2208	0.034	23 <sub>0</sub> <sup>1</sup> 26 <sub>0</sub> <sup>1</sup>
	2131	2066	0.040	25 <sub>0</sub> <sup>1</sup> 26 <sub>0</sub> <sup>1</sup>
	2215	2123	0.011	26 <sub>0</sub> <sup>2</sup>

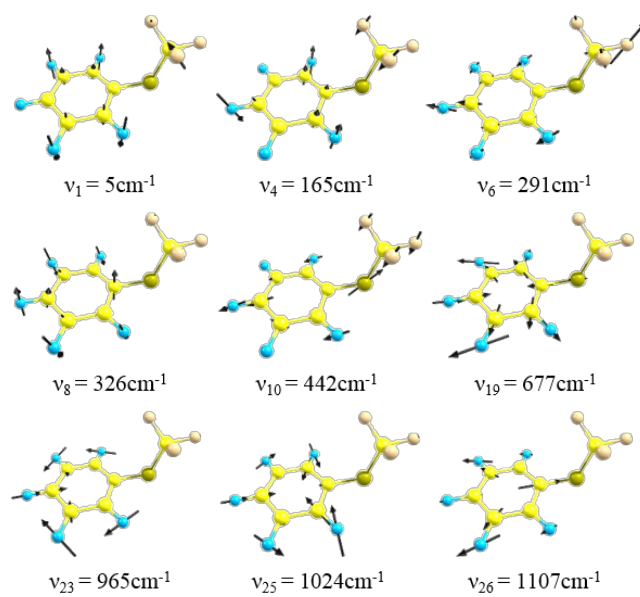
<sup>a</sup> The simulated values of Frank-Condon simulations using FClab II with the vibration frequencies obtained by SA3-CASSCF(12,11)/6-311<sup>++</sup>G(d,p) level of theory for S<sub>0</sub> and S<sub>1</sub>.

<sup>b</sup> The vibrational modes observed in the REMPI spectra are presented in Expt. column.

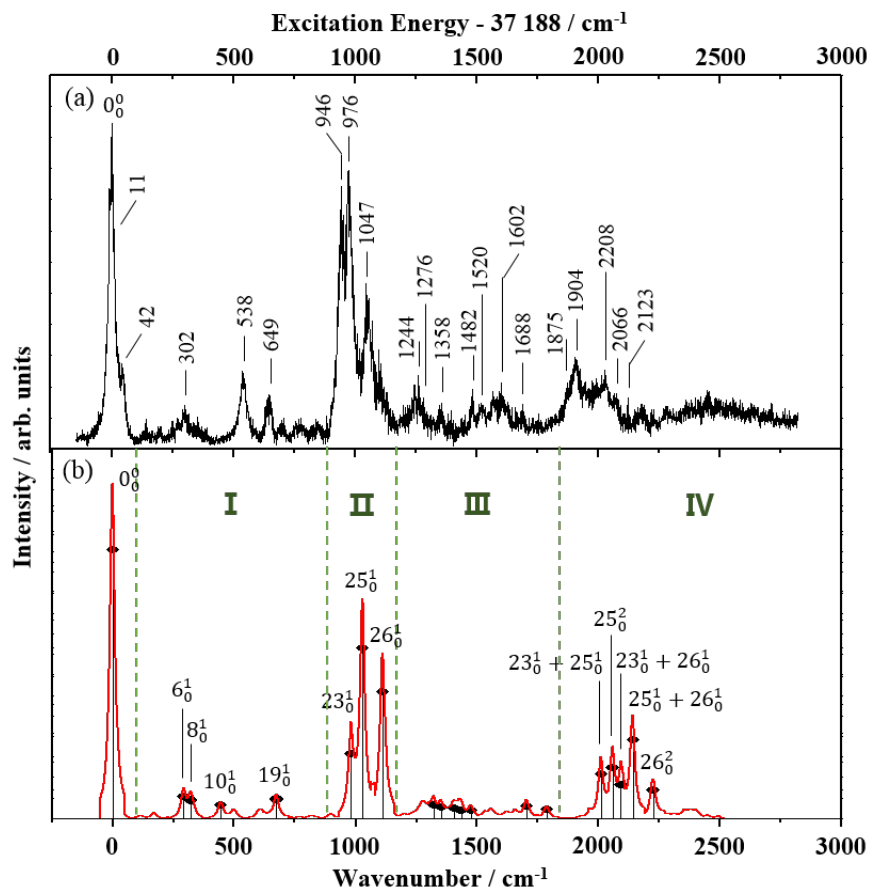
<sup>c</sup> Frank-Condon factors smaller than 0.003 are neglected.

<sup>d</sup> Assignments are described with the notation listed in increasing number for S<sub>1</sub> state.

<sup>e</sup> The  $\nu_6$  and  $\nu_8$  modes of S<sub>1</sub> state are unresolved in REMPI spectra and also, combination peaks of  $\nu_1$  and  $\nu_6$ .



**Figure S2.** Calculated normal mode eigenvectors of the five low-frequency out-of-plane vibrations ( $\nu_1$ ,  $\nu_4$ ,  $\nu_6$ ,  $\nu_8$ , and  $\nu_{10}$ ) and the four in-plane vibrations ( $\nu_{19}$ ,  $\nu_{23}$ ,  $\nu_{25}$  and  $\nu_{26}$ ) dominated in the  $S_1 \leftarrow S_0$  REMPI spectrum.



**Figure S3.**  $S_1 \leftarrow S_0$  REMPI spectrum of jet cooled (trifluoromethylthio)benzene(a) and Franck-Condon simulated spectra with appropriate vibrational mode assignment using unscaled SA4-CASSCF(12,11) vibrational frequencies(b).

**Table S5.** Theoretical frequencies and Franck-Condon factors observed in the simulated spectrum presented in Figure S2 (b).

	Calc. <sup>a</sup>	Expt. <sup>b</sup>	FC <sup>c</sup>	Assignment <sup>d</sup>
I	(0)	(31 788)	0.094	0 <sub>0</sub> <sup>0</sup>
	292	302 <sup>e</sup>	0.008	6 <sub>0</sub> <sup>1</sup>
	323		0.006	8 <sub>0</sub> <sup>1</sup>
	445	538	0.005	10 <sub>0</sub> <sup>1</sup>
	674	649	0.007	19 <sub>0</sub> <sup>1</sup>
II	981	946	0.023	23 <sub>0</sub> <sup>1</sup>
	1029	976	0.060	25 <sub>0</sub> <sup>1</sup>
	1112	1047	0.045	26 <sub>0</sub> <sup>1</sup>
III	1322		0.005	6 <sub>0</sub> <sup>1</sup> 25 <sub>0</sub> <sup>1</sup>
	1352		0.004	8 <sub>0</sub> <sup>1</sup> 25 <sub>0</sub> <sup>1</sup>
	1405		0.003	6 <sub>0</sub> <sup>1</sup> 26 <sub>0</sub> <sup>1</sup>
	1435		0.003	8 <sub>0</sub> <sup>1</sup> 26 <sub>0</sub> <sup>1</sup>
	1475		0.003	10 <sub>0</sub> <sup>1</sup> 25 <sub>0</sub> <sup>1</sup>
	1704		0.004	19 <sub>0</sub> <sup>1</sup> 25 <sub>0</sub> <sup>1</sup>
	1787		0.003	19 <sub>0</sub> <sup>1</sup> 26 <sub>0</sub> <sup>1</sup>
IV	2011	1904	0.016	23 <sub>0</sub> <sup>1</sup> 25 <sub>0</sub> <sup>1</sup>
	2059		0.018	25 <sub>0</sub> <sup>2</sup>
	2093	2208	0.012	23 <sub>0</sub> <sup>1</sup> 26 <sub>0</sub> <sup>1</sup>
	2142	2066	0.028	25 <sub>0</sub> <sup>1</sup> 26 <sub>0</sub> <sup>1</sup>
	2225	2123	0.010	26 <sub>0</sub> <sup>2</sup>

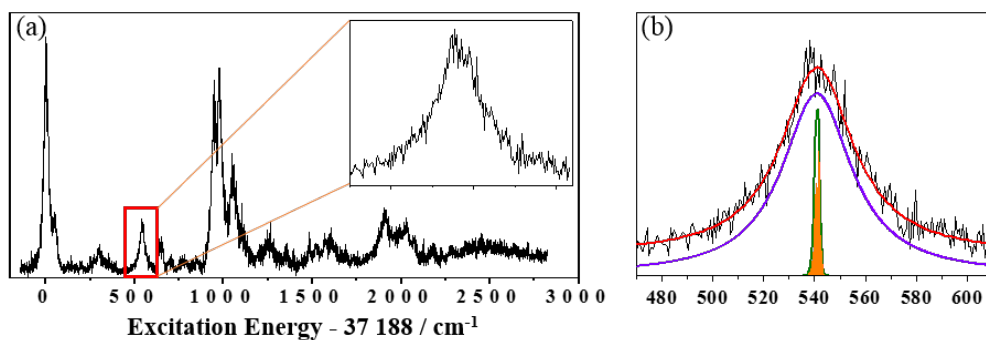
<sup>a</sup> The simulated values of Frank-Condon simulations using FClab II with the vibration frequencies obtained by SA4-CASSCF(12,11)/6-311<sup>++</sup>G(d,p) level of theory for S<sub>0</sub> and S<sub>1</sub>.

<sup>b</sup> The vibrational modes observed in the REMPI spectra are presented in Expt. column.

<sup>c</sup> Frank-Condon factors smaller than 0.003 are neglected.

<sup>d</sup> Assignments are described with the notation listed in increasing number for S<sub>1</sub> state.

<sup>e</sup> The ν<sub>6</sub> and ν<sub>8</sub> modes of S<sub>1</sub> state are unresolved in REMPI spectra.



**Figure S4.** (a) REMPI spectrum of (trifluoromethylthio)benzene. The peak at  $538\text{cm}^{-1}$  without spectral congestion is used to determine the lifetimes of the excited state. (b) Rotational contour (orange vertical drop line), simulated rotational structures with Gaussian width (green solid line), Voigt profile (violet solid line), and resulting convolution profile (red solid line)

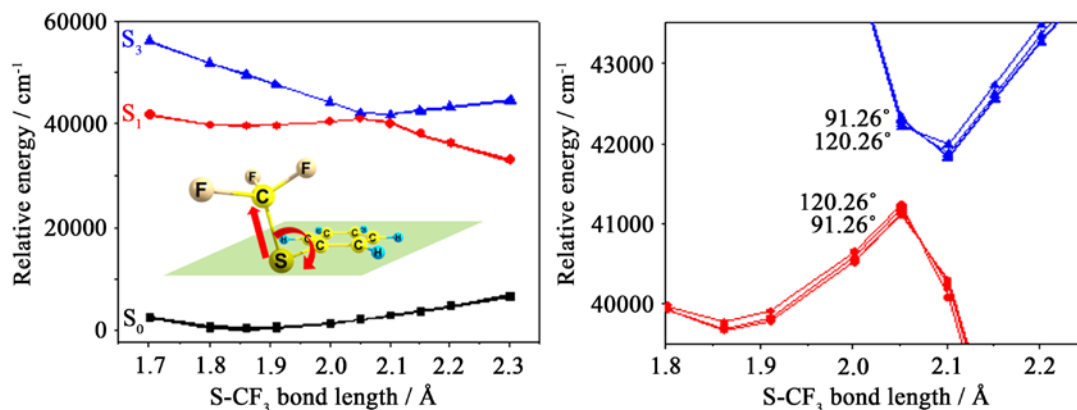
**Table S6.** Calculated rotational constants of (trifluoromethylthio)benzene for  $S_0$  and  $S_1$  states and fit parameters used in peak analysis. Excited state lifetime is given by the uncertainty principle with Lorentzian bandwidth.

Rotational Constants	$S_0$	$S_1$
A( $\text{cm}^{-1}$ )	0.07185	0.07020
B( $\text{cm}^{-1}$ )	0.01896	0.01866
C( $\text{cm}^{-1}$ )	0.18366	0.01805
$10_0^1 (6a)$		
Maximum of J	30	
T(K)	11	
Transition Type	a&b	
Gaussian FWHM( $\text{cm}^{-1}$ )	0.9	
Lorentzian FWHM( $\text{cm}^{-1}$ )	33	
Lifetime(fs)	322	

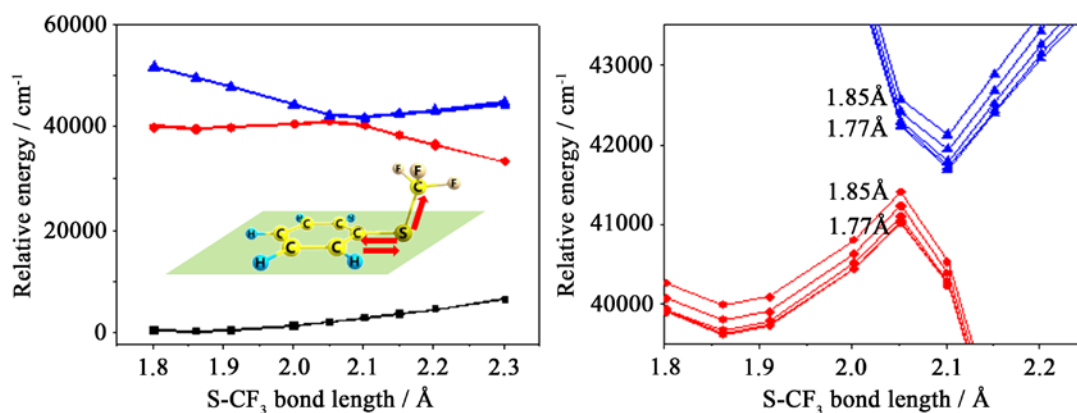
$$\text{FWHM (cm}^{-1}\text{) of Lorentzian fitted profile} = (\pi c \tau)^{-1} = \frac{10.62 \times 10^{-12}}{\tau \text{ (s)}}$$



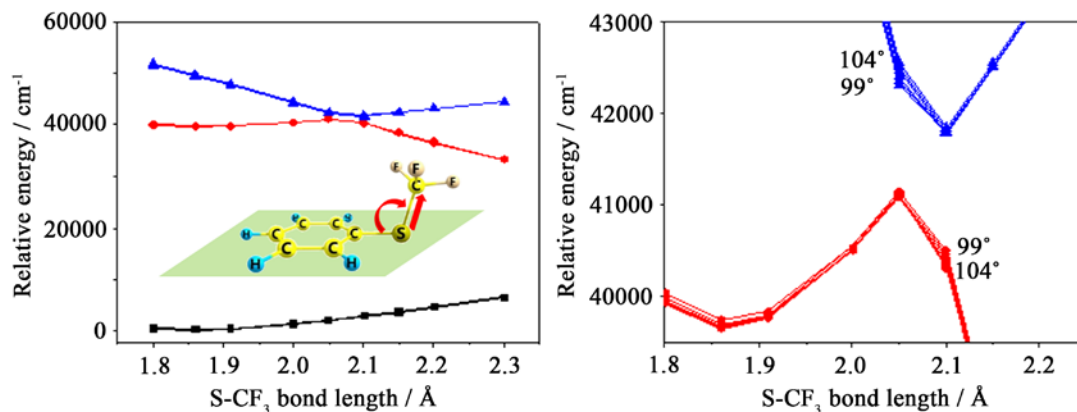
(a) S-CF<sub>3</sub> bond length and CCSC dihedral angle



(b) S-CF<sub>3</sub> bond length and C(ring)-S bond length



(c) S-CF<sub>3</sub> bond length and C(ring)-S-C angle



**Figure S5.** Three lowest ( $S_0$ ,  $S_1$ , and  $S_2$ ) adiabatic potential energy 2D cuts for three subcoordinates along S-CF<sub>3</sub> bond elongation obtained by SA3-CASSCF(12,11) level of theory; (a) CCSC dihedral angle, (b) C(ring)-S bond length, (c) C(ring)-S-C angle. (a) Each points on PES are obtained by fixing the S-CF<sub>3</sub> bond length and CCSC dihedral angle of 91.26 (CCSC dihedral angle of the minimum of the  $S_0$  state), 95.26, 100.26, 110.26, and 120.26°. (b) also obtained by fixing the S-CF<sub>3</sub> bond length and C(ring)-S bond length of 1.77, 1.79, 1.81 (C(ring)-S bond length of the minimum of the  $S_0$  state), 1.83, and 1.85 Å. (c) also obtained by fixing the S-CF<sub>3</sub> bond length and C(ring)-S-C angle of 99, 100, 100.81 (C(ring)-S-C angle of the minimum of the  $S_0$  state), 102, 103 and 104°. The region where  $S_1$  and  $S_2$  get nearer to each other are expanded in the right column to show the dependence between each two coordinates in detail.